Available online at www.sciencedirect.com
ScienceDirect
Quaternary International 161 (2007) 90–107

Late Pleistocene to Holocene marine transgression and thermohaline control on sediment transport in the western Magellanes fjord system of Chile (53°S)

Rolf Kilian[a,*], Oscar Baeza[a], Tatjana Steinke[a], Marcelo Arevalo[b], Carlos Rios[b], Christoph Schneider[c]

[a]*Department of Geology, FBVI, University of Trier, Behringstr., D-54296 Trier, Germany*
[b]*Instituto de la Patagonia, University of Magellanes, Casilla 113, Punta Arenas, Chile*
[c]*Department of Geography, RWTH Aachen University, Templergraben 55, D-52056 Aachen, Germany*

Available online 15 December 2006

Abstract

In the Western Strait of Magellan in southernmost Chile marine transgression occurred between 14,500 and 13,500 cal. BP. This is indicated by strongly increased accumulation of biogenic carbonate and first appearance of foraminifers in sediment records. From that time until 11,500 cal. BP, sedimentation in the western fjords became predominant autochthonous, due to higher salinity and clay flocculation, and Late Glacial glacier retreat. Present day thermohaline zonation pattern, extensively representative for the Holocene, and sedimentation rates indicate that westerlies hampered westward outflow of superficial (0–30 m water depth) glacial clay-rich freshwater from glaciated areas. During the Holocene, isostatic uplift of the Andes overcompensated sea level rise. In areas with high Glacial glacier loading this led to shallowing fjord sills and restricted exchange with marine water, especially since high freshwater inflow produced strong pycnoclines and preserved old saline water in fjord bottoms. To the east of the climate divide the Seno Skyring fjord system shows a year-round stable stratification, despite a strong wind-induced eastward superficial current in the upper 30–50 m of the water column. Such currents enabled significant Late Glacial eastward transport of glacial clay. Sediment cores from this area indicate that east-ward sediment flux slowed down during the Holocene, probably due to less intense westerlies. Investigated present day thermohaline characteristics of the fjord system across the superhumid climate divide of the Southern Andes indicate details of the exchange between marine and freshwater which are fundamental for evaluation of sediment transport pathways, biogenic productivity and interpretation of paleoclimate records in this area.

1. Introduction

From 42° to 55°S, the Pacific margin of South America represents a 200–300 km wide shelf with thousands of islands and a fjord system across the Andes (Figs. 1 and 2). During the Last Glacial, most of these fjords were proglacial lakes. At some time after the Last Glacial Maximum (LGM) the global sea level rise (e.g. Bard et al., 1996) led to marine transgression into the continental margin (Clapperton et al., 1995; Anderson and Archer, 1999; Brambati, 2000; McCulloch et al., 2005b; Sudgen et al., 2005). Only fragmentary information exists of this coastal zone (Escribano et al., 2003; Acha et al., 2004), where large amounts of freshwater mixes with Pacific marine water (Strub et al., 1998; Dávila et al., 2002). Varying terrestrial input of sediments and organic matter, and its complex distribution by fjord currents, led to partly high bioproductivity and biodiversity (Mann and Lazier, 1996; Arntz and Ríos, 1999; Escribano et al., 2003). High amounts of freshwater and sediment come from the southernmost Andes which represent one of the most pronounced climate divides in mid- to high latitudes with annual precipitation exceeding 10,000 mm/yr (Schneider et al., 2003). Tidal currents, fjord bathymetry and

*Corresponding author. Tel.: +49 651 2014644; fax: +49 651 2013915.
E-mail addresses: kilian@uni-trier.de (R. Kilian), carlos.rios@umag.cl (C. Rios), christoph.schneider@geo.rwth-aachen.de (C. Schneider).

1040-6182/$ - see front matter © 2006 Elsevier Ltd and INQUA. All rights reserved.
doi:10.1016/j.quaint.2006.10.043

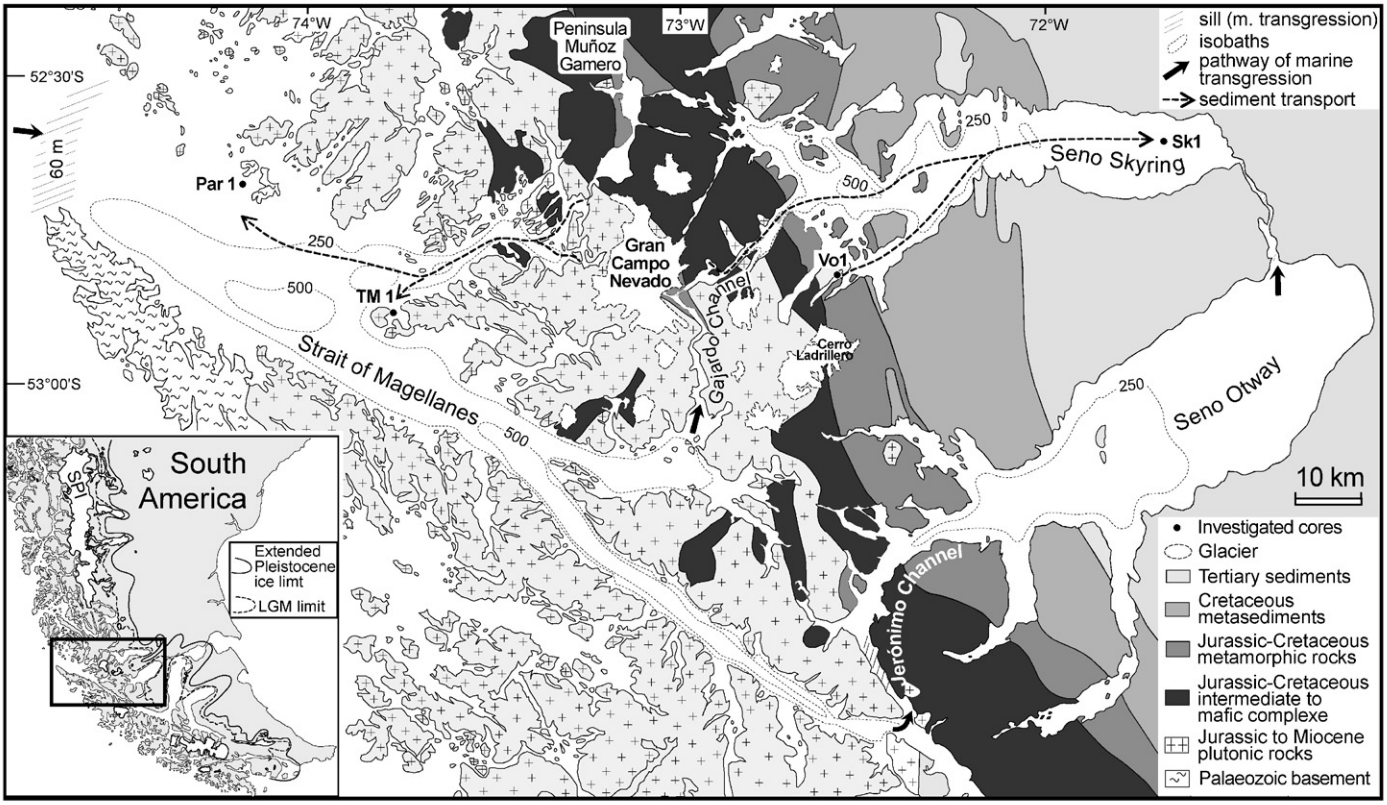

Fig. 1. Generalised geological map (modified after SERNAGEOMIN, 2003) of the southern Andes between 52 and 53°S with locations of sediment cores PAR1, TM1, VO1 and SK1. Possible sediment fluxes from the elevated Gran Campo Nevado and Cerro Ladrillero areas into the foreland fjord system to the east and west are indicated by arrows with dashed lines. Sills which controlled marine transgression are shown. Note the Jurassic to Cretaceous intermediate to mafic metamorphic belt in the central part of the Andes which could have introduced chlorite- and magnesium-rich sediments into the Seno Skyring fjord system.

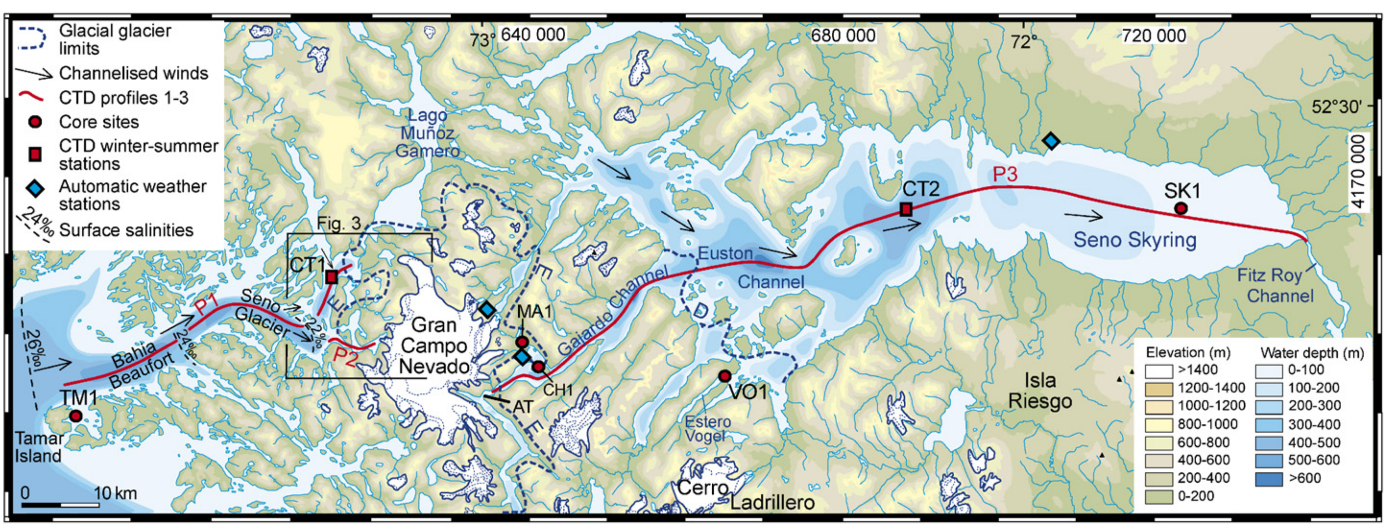

Fig. 2. Topographical and bathymetrical characteristics of Gran Campo Nevado and Seno Skyring area with UTM grid (Geodetic datum: South America 69) from Kilian et al. (in press). The location of salinity, temperature and oxygen profiles (P1–P3), single CTD stations (CT1 and CT2), surface salinities in the western section and mentioned drilling sites (of sediment cores TM1, VO1, SK1, MA1 and CH1) are indicated. Stippled lines indicate glacier limits D at ~15,000 and E at ~12,000 cal. BP after Kilian et al. (in press). Locations of three automatic weather stations, which have been considered with respect to the hydrological budget, are indicated (Schneider et al., 2003).

predominant westerly winds control the mixing process between freshwater and Pacific water. Thermohaline structure and circulation in the fjord systems (e.g. Panella et al., 1991) and associated sediment transport are widely unexplored and may have changed also fundamentally after the marine transgression. Based on sediment cores from the Magellan and Skyring fjord system (Fig. 1) this paper aims at constraining the Late Glacial marine transgression and associated changes in accumulation of terrigeneous and biogenic sediment components since the LGM.

At present, several glaciers of the southern Andes reach a fjord system and introduce clay and freshwater plumes. Superficial wind-induced currents may play an important role for the distribution of these sediments (e.g. Matsuura and Cannon, 1997; Stow and Tabrez, 1998; Valle-Levinson et al., 2001; Valle-Levinson and Blanco, 2004). The sedimentation process of clayey suspension is also controlled by flocculation processes and the settling velocity of clay minerals which depends on salinity, water temperature, biopolymer concentration, turbulent shear and suspended solid concentration of the estuarine fjord system (e.g. Aston, 1978; Dyer, 1989; Van Leussen, 1999; Parsons and Garcia, 2000; McCool and Parsons, 2004). In this context our paper introduces present day thermohaline characteristics and oxygen loading of a 160 km long fjord system across the super-humid climate divide of the Andes (Figs. 1 and 2) which are fundamental for evaluation of sediment pathways, biogene productivity and interpretation of paleoclimate records in this area.

2. Regional setting

Most fjords of the considered transect through the continental margin in southernmost Chile originate from the 200 km^2 Gran Campo Nevado (GCN) Ice Cap (Schneider et al., in press) with a maximum elevation of 1750 m, located at 53°S on the southern Península Muñoz Gamero (Fig. 1). It represents a remnant of the Southern Patagonian Icefield (SPI) (see inset to Fig. 1; e.g. Mercer, 1976; Hollin and Schilling, 1981). At present, several glaciers of the GCN reach the fjord system and produce extended clay fans (Fig. 3). During the LGM large glacier systems extended 110 km to the east and west. A major glacier system flowed from GCN to the west through Swett Channel, Seno Glacier and Bahia Beaufort until a shallow sill (60 m deep at present) close to the western entrance of the Strait of Magellan (Figs. 1–3). Due to a 120 m deeper sea level at LGM the coastline was 30 km further to the west, so that the glaciers drained through fluvio-glacial streams towards the Pacific. Ice recession left behind a proglacial lake system with water depths of >520 m (Fig. 1). The sediment cores PAR1 and TM1 were taken along this fjord system (Figs. 1 and 2) to document the history of deglaciation and marine transgression.

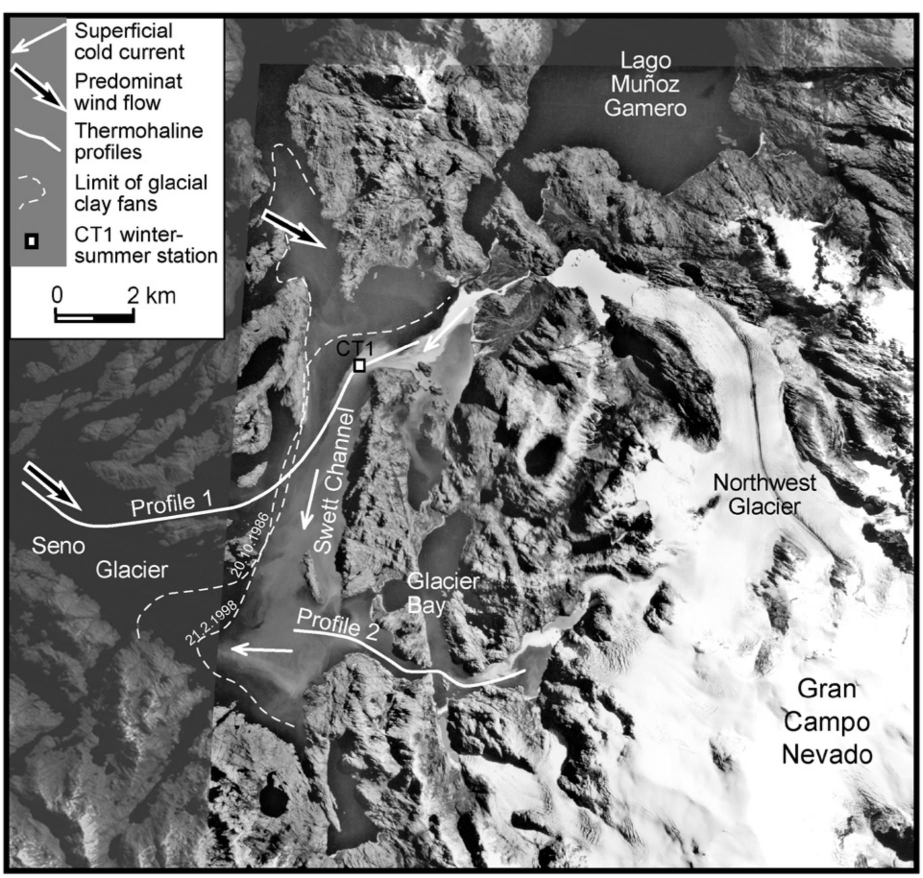

Fig. 3. Aerial photograph of the eastern section of Gran Campo Nevado (21.2.1998; Schneider et al., in press) with the Swett Channel and typical extend of glacial melt water fans, documented at 20.10.1986 and 21.2.1998 (stippled white lines). Orientation of CTD Profiles 1 and 2 as well as predominant wind directions (black arrows; Schneider et al., 2003) and superficial cold water flows (white arrows) are shown.

At present, Swett Channel is influenced by several outlet glaciers of GCN and the outflow of Lago Muñoz Gamero which together introduce several hundreds of m^3 freshwater per second (Fig. 3; Marangunic et al., 1992). A large glacier outflow fan originates from the 12 km long Northwest Glacier of GCN (Fig. 3), where we measured sediment loads of 30–40 mg/l. The predominant north-western winds are channelised and displace the glacial melt water plume typically towards the south, where it mixes with additional glacial melt water of the Glacier Bay (Fig. 3). Sediment loads in the southern section of Seno Glacier and Swett Channel drop to <10 mg/l and further to the west-northwest it becomes undetectable, indicating rapid clay settling, possibly due to flocculation processes in more saline water (e.g. Dyer, 1989; Winterwerp, 1998).

To the east of GCN a major LGM glacier pathway was through the north-eastern Gajardo and Euston Channels, where it merged large glaciers coming from Cerro Ladrillero, and continued until the eastern shores of Seno Skyring (Fig. 2). This fjord system has a restricted marine influence. The sediment cores VO1 and SK1 were obtained from this area to document changes since the LGM.

Pronounced lithological changes of the basement rocks occur across the focussed Andean transect (Fig. 1). Therefore mineralogical and chemical characteristics of sediments can be used to constrain sediment pathways. Similarly, the amount of mafic Andean detritus transported towards the Pacific coast has been investigated by means of chemical tracers further north at 40°S by Lamy et al. (2004).

3. Materials and methods

3.1. Echo sounding, bathymetry and sediment cores

The fjord bathymetry was investigated by a Parametric Echo Sounding System SES 96 from Innomar (Wunderlich and Wendt, 2001) which has a depth range up to 800 m with a maximum vertical resolution of <5 cm. Water depths were calculated from the high frequency signal, which was calibrated with water density profiles calculated from water temperatures and salinities (Chapter 2.3).

Sediment structures (up to 50 m sediment depth) and depth of tephra layers were investigated systematically with the SES 96 echo sounding, using low frequency signals of 4–12 kHz. Drilling localities were selected after the sediment echo sounding profiles. Sediment cores were taken with a 5 m long Uwitec piston corer (6.5 cm diameter; for location see Fig. 1) with the RV *Gran Campo II* between March 2002 and October 2004 (Kilian et al., in press). Here we concentrate on four sediment cores along the fjord transect, which document the last 20,000 years.

In the western fjord section, 30 km east of the western entrance of the Strait of Magellan, the 4.6 m long sediment core PAR-1 was taken in 32 m water depth south of Parker Island (Figs. 1 and 2). The 7.2 m long sediment core TM1 was obtained in 31 m water depth, approximately 30 km southeast of this location, near Tamar Island.

A 4.7 m long core (SK1) was obtained from the eastern section of Seno Skyring in 72 m water depth and >8 km from the nearest shoreline (Figs. 1 and 2). The flat slopes of this basin may have precluded turbidites and coarse clastic sediment input. Also in the Skyring area, a 4.6 m long core (VO1) was obtained in 37 m water depth at the north-eastern end of fjord of Estero Vogel, an ancient glacial valley, originating at Cerro Ladrillero (Fig. 1). Paleoclimate interpretations of the cores VO1 and SK1 are published in Kilian et al. (in press). We concentrate here on their implications on long-distance sediment transport.

3.2. Salinity, temperature and oxygen determination

Salinity, temperature, depth (CTD) and oxygen were measured in March 2003 and August 2004 with the CTD sensor (Model SD204) of SAIV A/S Environmental Sensors and System. The salinity range of the measurement device is between 0‰ and 40‰ with a resolution of 0.01‰ and an accuracy of ± 0.02‰. The temperature range is between –2 and +40 °C with a resolution of 0.001 °C, an accuracy of ± 0.01 °C and a response time of 0.5 s. Water depths were measured with a pressure sensor which has a resolution of 0.01 dbar (m) and an accuracy of ± 0.02%. The dissolved oxygen was determined with the sensor type SAIV205 in the range 0–20 mg/l with a resolution of 0.01 mg/l and an accuracy of ± 0.2 mg/l. Salinity and temperature data were also used to calibrate echo sounding data. Thermohaline profiles and isolines were performed with the Ocean View Data Programme (Schlitzer, 2004).

3.3. Age determination

Measurements of ^{14}C were done by accelerator mass spectrometry (AMS) in Poland. The activity of ^{14}C was determined from acid extracts of terrestrial macrofossils from the sediment cores. $^{13}C/^{12}C$-ratios were measured simultaneously and used to correct mass fractionation. Conventional ^{14}C-ages were calibrated using the CalPal 2005 SFCP curve, which is identical to the Intcal04 calibration curve (Stuiver et al., 1998; see http://www.calpal.de/calpal/manual/CalCurves/CalPal2005_SFCP.htm for further details). It is suggested that this is the best available calibration curve at present, because it considers the most important recent calibrations for different time intervals. All depicted ages are means of one-sigma values. Calibrated ^{14}C ages referred to in the text and in Fig. 4 are listed together with radiocarbon ages in Table 1. All cited ^{14}C ages, which were used for comparison, have also been recalculated with *Calpal* 2005. A mean reservoir age of 400 years was estimated for the Pacific at 40°S (Bard, 1988; Lamy et al., 2004). However, there are no constraints for the regional reservoir effect in the investigated fjord zone which is characterised by a pronounced pycnocline and high amounts annual fresh water addition (>6 m yearly

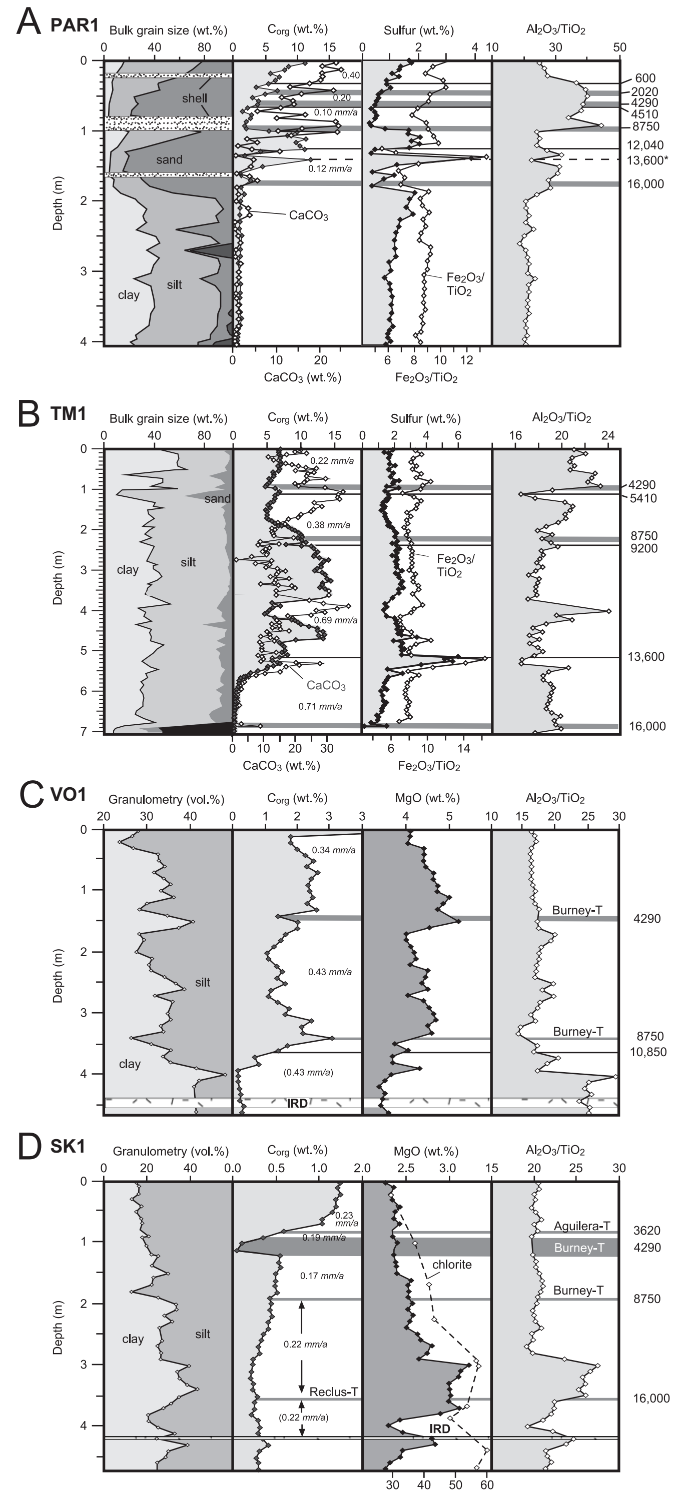

Fig. 4. Selected chemical and mineralogical parameters (grain size, C_{org}, biogenic carbonate, sulphur, MgO contents, and Al_2O_3/TiO_2 and Fe_2O_3/TiO_2 ratios) of sediment cores PAR1 (A) near Parker Island and TM1 (B) near Tamar Island in the western entrance of the Strait of Magellan, and VO1 (C) and SK1 (D) from Seno Skyring fjord system east of GCN (locations see Figs. 1 and 2). Calibrated ^{14}C AMS ages from shell (200 years reservoir age) and macroplant relicts are given as black lines and identified tephra layers are shown as thick grey lines together with their ages (details see Table 1). An age marked with * in PAR1 (A) is adapted from TM1 core (B) where the pronounced sulphur peak was dated. Sedimentation rates (in mm/a) are given for specific core segments.

precipitation), suggesting a lower reservoir age. The relationship of ^{14}C ages to well-dated tephra layers is in agreement with a reservoir age of 200 years (Table 1).

^{210}Pb ages were calculated from ^{210}Pb, ^{214}Pb and ^{226}Ra activities of six samples from the upper 14 cm of the sediment core PAR1. Sediment ages are calculated after the CRS model which assumes a Constant Rate of ^{210}Pb Supply (Appleby et al., 1979). For further details, see Hagedorn et al. (1999).

Tephra layers found in all sediment cores are time markers. Tephra and glass was separated, even if macroscopically not visible. The morphological characteristics of glass shards and pumice fragments were investigated with a Leo Scanning Electron Microscope (SEM) LEO 435 VP at the University of Trier and compared with separates from well determined tephra layers from previously investigated sediment and peat cores from the area (Kilian et al., 2003). In ambiguous cases the chemical composition of the glass was determined by an electron microprobe (Cameca SX51 at University of Heidelberg), equipped with five wavelength dispersive spectrometers, using an accelerating voltage of 15 kV and a beam current of 20 nA. The electron beam diameter was focused to ~1 μm for most minerals, ~5 μm for feldspar and 5–20 μm for glass. Natural and synthetic minerals were used for calibration. The glass composition was compared with the composition of well determined tephra layers from eruptions of the volcanoes Burney, Reclus, Aguilera and Hudson (Kilian et al., 2003). Ages and depths of tephra layers determined in different sediment cores are listed in Table 1.

3.4. Granulometry and mineralogy

The particle size analyses were made with a Galai CIS-1 laser particle counter with an analytical range between 0.5 and 150 μm. About 50 mg of air-dried sediments were dissolved in 50 ml distiled water. The organic material was removed with a solution of H_2O_2 (10%) over a period of 15 h. Afterwards samples were placed in a water bath at 60–70 °C. Finally, the samples were treated in an ultrasonic bath for 20 min before being measured with the particle analyzer. The considered ranges of particle sizes are 0.5–2 μm (clay), 2–63 μm (silt) and 63–150 μm (fine sand). Clay minerals were investigated in textural supplements of the separated clay fraction (<2 μm) by X-ray diffractometry with a Siemens D500 diffractometer at the University of Trier and at the Alfred-Wegener-Institute Bremerhaven, Germany.

3.5. Chemical analysis

Major and some trace elements (e.g. Sr, Ba, Zr) have been measured by Atomic Absorption Spectrophotometry (AAS; Perkin-Elmer). About 100 mg of sediment were dried (105 °C) and fused in Platinum skillets with 400 mg of a flux material (mixture of Lithiumtetraborat, Lithiumcarbonate and Lanthanoxide). Produced glass pearls were

Table 1
Tephrochronological data, including source volcanoes, depth of tephra layers in sediment cores PAR1, TM1, VO1, SK1 and tephra ages with references

Volcano	Depth of tephra layer in different sediment cores	^{14}C age BP	Calibrated age BP (Calpal2005)	Averages of min–max-ages	References
Tephrochronology					
Mt. Burney	21 cm in PAR1	1940 ± 30–2170 ± 30	1830 ± 40–2210 ± 90[(a)]	2020 ± 90	(a) Biester et al. (2002) 1980 ± 40–2060 ± 90[(b)]
	(b) Kilian et al. (2003)				
Aguilera	83 cm in SK1	< 3345 ± 195	< 3620 ± 230		Stern (1990)
Mt. Burney	44 cm in PAR1; 96 cm in TM1; 96-118 cm in Sky1, 146–148 in VO1	3860 ± 50	4290 ± 90		McCulloch and Davies (2001)
Mt. Burney	192–194 cm in SK1; 225 cm in TM1; 343 cm in VO1	< 7890 ± 45			8370 ± 270–9220 ± 300[(a)]
8750 ± 110	(a) Stern (1992, 2000)				
			8750 ± 110[(b)]		(b) Kilian et al. (2003)
Reclus	172 in PAR1; 356 cm in SK1; 695 cm in TM1				12,870 ± 200–13,260 ± 210
	15,720 ± 630–16,280 ± 600	16,000 ± 630	Stern (1992, 2000)		
Radiocarbon ages					
Soil and sediment core	Depth and material	^{14}C age	Calibrated age BP (Calpal2005)	Comment	References
Soil Otway spillway	Organic material	12,460 ± 190	14,680 ± 420	Deglaciation of Jeronimo Ch.	Mercer (1970)
TAM1	104 cm (shell)	4870 ± 40	5410 ± 60	Reservoir time of 200 years for shell	This paper
	238 cm (shell)	8430 ± 50	9200 ± 80		This paper
	524 cm (shell)	11,720 ± 60	13,420 ± 120		This paper
VO1	365 cm (leaf)	9490 ± 50	10,850 ± 160		This paper
PAR1	31 cm (shell)	800 ± 30	600 ± 40	Reservoir time of 200 years for shell	This paper
	67 cm (shell)	4240 ± 35	4510 ± 50		This paper
	125 cm (macroplant remains)	10,260 ± 50	12,040 ± 190		This paper

Additionally, uncalibrated and calibrated radiocarbon ages (CalPal2005) and calculated marine reservoir ages are given.

dissolved in 40 ml HCl (0.5 N). Liquids of samples and international standards (MRG-1, SY-2 and JG-2) were measured by AAS. Determined major elements, loss on ignition (1050 °C), and independently detected contents of CO_2 and SO_2 resulted in sums of 99–101 wt%. For comparison of major element contents, analyses were normalised to volatile-free. Carbon, sulphur and nitrogen concentrations were determined by means of a C/S-Analyser (ELEMENTAR) burning 10–20 mg sample aliquots in a tin capsule. Mean relative standard deviations were 2.2% for C, 2.1% for S and 2.1% for N. Estimated detection limits were 0.01 wt% for carbon, 0.02 wt% for sulphur and 0.02 wt% for nitrogen.

3.6. Scanning electron microscopy

The texture of minerogenic (e.g. quartz, framboidal pyrite) and biogenic components (e.g. diatoms, foraminifers), and volcanic tephra in the sediments were determined at Trier University with a scanning electron microscope (SEM) LEO 435 VP. Sediment samples were air-dried and spattered with gold within the Polaron Equipment Sem coating unit E5000. Morphological characteristics of sediment components were investigated in secondary electron images. Chemical composition of components was determined with the Energy Dispersive X-ray Analyzer (*Link Analytical eXL*).

4. Results

4.1. Bathymetry, hydrology and sediment load

Approximately 1600 km of echo sounding profiles were obtained from the investigated transect. High frequency signals were calibrated with the CTD profiles (locations in Fig. 2) to determine bathymetry which is roughly shown in Fig. 2. Especially, water depths of sills were determined to constrain in- and out-flow properties. Low frequency echo signals of 4–12 kHz show sediment characteristics along the fjord transect. The pronounced 4290 cal. BP tephra layer of Mt. Burney was identified in nearly all echo sounding profiles. At the drilling sites the discrepancy between the depth of the tephra layer (using sound velocities of the marine water) and the depth in the sediment core were less than 5%. This allows estimation of sedimentation rates and their regional changes. Near GCN in the Swett Channel (Fig. 3) this tephra layer appears in 3–10 m sediment depth, corresponding to sedimentation rates of 0.7–2.6 mm/yr. Echo sounding profiles taken 40 km to the east near to Tamar Island (Fig. 2) show the Mt. Burney tephra layer in

1–3 m depth, suggesting sedimentation rates of 0.2–0.7 mm/yr. 40 km further to the east, near Parker Island at the western entrance of the Strait of Magellan (Fig. 1), the Mt. Burney tephra is very thin and difficult to detect in echo sounding profiles. However, in most profiles it appears in less than 0.4 m sediment depth, suggesting sedimentation rates of less than 0.1 mm/yr.

Sediment echo sounding profiles of the Gajardo Channel and Euston Channel near GCN (Fig. 2) show 36 m of fine-grained and well-sorted Late Glacial and Holocene sediments. The 4290 cal. BP Mt. Burney layer was identified in 4–10 m sediment depth suggesting sedimentation rates of 0.8–2.6 mm/yr. Along the Seno Skyring and towards the east, the sediment depths in which the tephra layer of Mt. Burney appears, decrease systematically from 4 to less than 1 m. This suggests continuously decreasing sedimentation rates from west to east, i.e. from 0.8 to less than 0.2 mm/yr.

For better interpretations of the thermohaline profiles of Seno Skyring, the water level in the Gajardo Channel was monitored by an automatic gauge station around 10 km northeast of Angostura Tempanos (AT in Fig. 2) from April 1, 2002 to February 28, 2003. Precipitation was an important factor controlling the fjord water level ($r = 0.65$) which showed maximum changes of ± 0.40 m compared to an average fjord level, while wind and tides produced only minor water level fluctuations of ± 0.05 m. In Euston Channel and western Seno Skyring precipitation also dominates the water level, while tidal influences are absent. Along the eastern shores of Seno Skyring the intensities of westerlies control the lake level, which can increase to 1 m above long-term average, while tidal influences are restricted to less than 10 km distance from the entrance of Fitz Roy Channel (Marangunic et al., 1992).

4.2. Sediment records

Stratigraphy of the 4.1 m long PAR1 sediment core from the western entrance of the Strait of Magellan (locality shown in Fig. 1) is based on ^{210}Pb and ^{14}C ages and tephrochronology (Fig. 4A and Table 1). The relationship between sediment core depth and the ages is shown in Fig. 5.

Calculated ^{210}Pb ages are 0 years before 2005 at 1 cm, 8 years at 3 cm, 15 years at 7 cm, 38 years at 7 cm, 119 years at 9 cm, 122 years at 11 cm and 139 years at 13 cm, indicating that the sediment surface was recovered. The stratigraphy of the soft superficial sediment is likely to have been slightly disturbed before sampling, which could explain the variations in the ^{210}Pb sedimentation rates from 0.5 to 1 mm/yr. Compared to the Early Holocene and Late Glacial, this relatively high sedimentation rates are largely related to the extreme high water content (>85 wt%) in the uppermost core section.

The tephra layer of the 2020 cal. BP eruption of Mt. Burney occurs at 41 cm core depth and a second

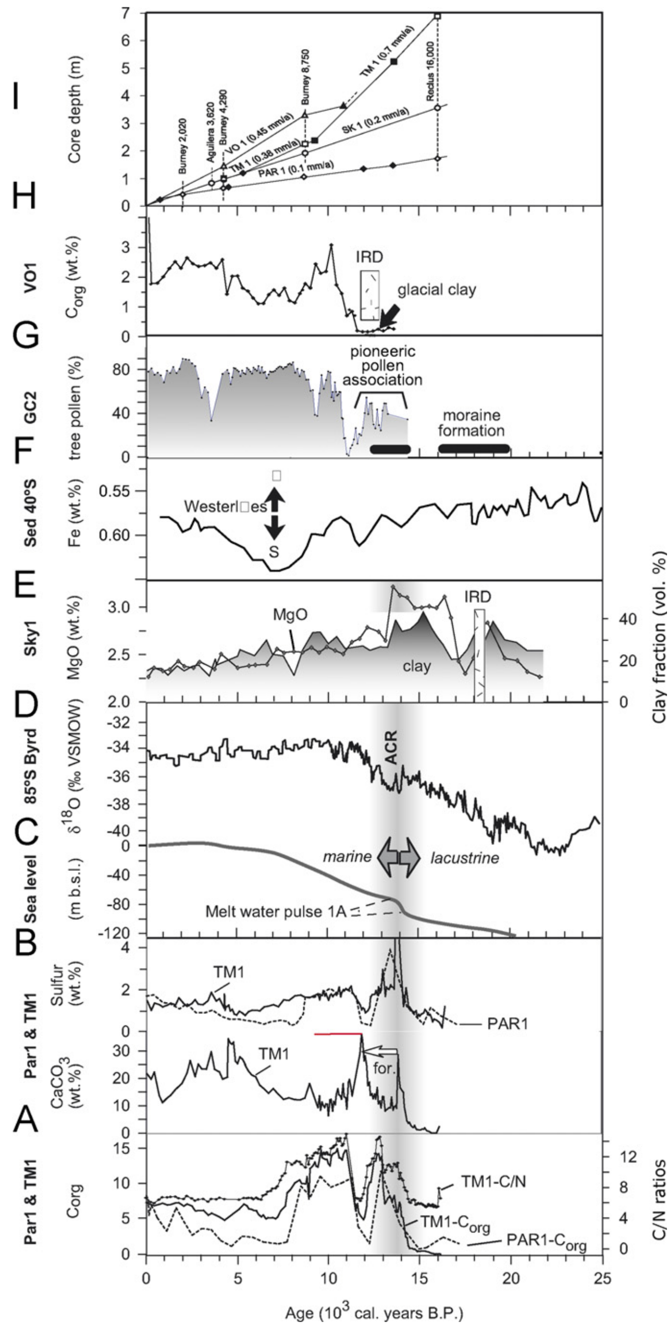

Fig. 5. (A) Changes of C_{org} and C/N ratios in sediment core PAR1 and (B) a comparison of sulphur und biogenic $CaCO_3$ contents in PAR1 and TM1 cores (C). Global sea level curve (Bard et al., 1996, modified after Rohling et al., 2004) and (D) δ^{18}O values from Byrd ice core (Blunier and Brook, 2001) are plotted for the last 25,000 years. (E) MgO contents and vol% of clay fraction from the sediment core SK1 are compared to (F) Fe concentrations in sediments from the Chilean shelf north of 40°S at the northern margin of the westerly zone with deduced westerly shifting (Lamy et al., 1999). (G) Tree pollen from peat core GC2 from Bahia Bahamondes in Gajardo Channel (Fesq-Martin et al., 2004) and (H) C_{org} in VO1 sediment core document forest expansion (IRD: ice rafted debris). (I) Sediment core depths (in m) vs. tephra and ^{14}C ages for investigated cores together with sedimentation rates (in italics).

tephra layer of the 4290 cal. BP eruption of Mt. Burney at 63 cm core depth (Fig. 4A and Table 1), constraining sedimentation rates of 0.40 and 0.20 mm/yr for this uppermost sections. The 8750 cal. BP Mt. Burney tephra layer appears at 98 cm sediment depth.

Radiocarbon ages of shell were obtained from 31 cm depth (600 ± 40 cal. BP), from 67 cm depth (4510 ± 50 cal. BP) and from 125 cm core depth (12,040 ± 190 cal. BP). This indicates lower sedimentation rates from the Late Glacial (0.10 mm/yr) compared to the Late Holocene (up to 0.4 mm/yr). This can be partly explained by strongly increasing water content and frequent sand layers of short events in the uppermost 100 cm of the core until the sediment surface (from <40 to >85 wt%).

PAR1 shows one pronounced sulphur peak at 135–140 cm core depth (Fig. 4A). A similar sulphur peak appears in the TM1 core (Fig. 4B) for which a leaf gave an age of 13,420 ± 120 cal. BP. An additional tephra in PAR1 appears at 171–172 core depth and was related to the 16,000 cal. BP eruption of Reclus Volcano (Table 1; Stern, 1992; Kilian et al., 2003). However, the radiocarbon ages between 12,500 and 13,100 have large uncertainties due to flat ^{14}C calibration curves (see www.calpal.de). Based on profiles along the Strait of Magellan McCulloch et al. (2005a) have discussed and proposed a lower age range of 15,510–14,350 cal. BP for this Reclus tephra. Using the latter ages, the sediment cores discussed here would have lower sedimentation rates in the Late Glacial compared to the Early Holocene which seems not very reasonable. In PAR 1 the Reclus tephra indicates sedimentation rates of 0.12 mm/yr for the period between around 16,000 and 13,000.

The Glacial sediment section of PAR1 (>16,000 cal. BP, below 170 cm core depth) is characterised by very low C_{org} (<1 wt%), low biogenic carbonate (<1 wt%, except for a shell layer at 210–220 cm core depth) and relatively high amounts of clay (30–40 wt%; Fig. 4A). Above 170 cm core depth grain sizes become coarse and several sandy shell-rich layers appear (Fig. 4A). Below 200 cm core depth Al_2O_3/TiO_2 ratios are relatively low (19–22) and similar to those of the granodioritic Patagonian Batholith in the GCN area (Fig. 1). Above 200 cm core depth Al_2O_3/TiO_2 ratios increase significantly from 20 to >26, indicating a change in sediment source lithologies.

Foraminifers occur above of 150 cm core depth, where biogenic $CaCO_3$ contents first reaches more than 5 wt%. Between 150 and 135 cm core depth (corresponding to 14,500–13,500 cal. BP; Figs. 4A and 5A, B) C_{org} contents increase strongly from 1 to >10 wt% and a pronounced sulphur peak (~4 wt%) together with high Fe/Ti ratios and high amounts framboidal pyrite appear (Fig. 4A).

Stratigraphy of TM1 core (locality see Figs. 1 and 2) is based on a tephra layer of the 4290 cal. BP eruption of Mt. Burney Volcano at 95 cm core depth, a tephra of the 8750 cal. BP eruption of Mt. Burney at 225 cm depth and a tephra layer of the 16,000 cal. BP eruption of Reclus at 690 cm (Fig. 4B and Table 1). ^{14}C ages from shell were obtained from 104 cm (5410 ± 60 cal. BP) and from 238 cm (9200 ± 80 cal. BP). A leaf from 524 cm core depth (13,420 ± 120 cal. BP) was sampled around 2–3 cm above the pronounced sulphur peak (6 wt% S; Fig. 4B). The lowest sedimentation rates of 0.22 mm/yr occur in the uppermost section between 0 and 104 cm core depth and are somewhat higher (0.38 mm/yr) in the middle and early Holocene section between 104 and 225 cm core depth (Fig. 5). The predominant Pleistocene core section below 225 cm depth shows the highest sedimentation rates of ~0.7 mm/yr (Figs. 4B and 5).

The lowermost core section (710–590 cm core depth) is characterised by very low C_{org} (>1 wt%) and $CaCO_3$ contents (<1 wt%), and low C/N ratios (6–7; Fig. 5A). Strong increases of biogenic $CaCO_3$ (from <3 to 28 wt%) and C_{org} (from <2 to >7 wt%) occur between 590 and 520 cm core depth (Fig. 4B), corresponding to 14,500–13,500 cal. BP. This core section is also characterised by a pronounced sulphur peak and extraordinary high Fe_2O_2/TiO_2 ratios similar to that of PAR1 at 135 cm depth (see Figs. 4 and 5). Above 540 cm core depth first foraminifers were found. Between 520 and 430 cm core depth biogenic $CaCO_3$ contents are just 10–15 wt%. A second $CaCO_3$ peak (35 wt%) occurs between 430 and 380 cm core depth, corresponding to 12,000–11,000 cal. BP (Fig. 5B). During the Holocene (above 3.5 m core depth) $CaCO_3$ contents increase continuously until around 4500 cal. PB (130–110 cm core depth) while the values decrease again until at least 1000 cal. BP (20 cm core depth). From 480 to 440 cm core depth (13,000–12,100 cal. BP) C_{org} contents reach 12 wt%, from 420 to 380 cm core depth (12,000–11,000 cal. BP) C_{org} drop to ~5 wt% and from 360 to 280 cm core depth (10,800–9500 cal. BP) C_{org} increases again to around 12 wt%. From 280 to 180 cm core depth (9500–7200 cal. BP) C_{org} decreases continuously until 5 wt% and then remains at this level up to the sediment surface. The increase in Corg is accompanied by an increase of C/N ratios (from 6 to 16; Fig. 5A). TM1 and PAR 1 show similar C_{org} patterns (Fig. 5A).

Clayey sediments with Al_2O_3/TiO_2 ratios (18–22), similar to those of the Patagonian Batholith and Late Glacial sediments of PAR1, are typical for the lowermost TM1 core section below 580 cm, suggesting a predominant allochthonous sediment origin from the GCN area (Fig. 1).

VO-1 core (Fig. 4C) from Estero Vogel north of Cerro Ladrillero (Fig. 2), consists of clayey to silty sediments and includes a tephra layer of Mt. Burney (4290 cal. BP) at 146–148 cm depth. An early Holocene tephra of Mt. Burney (8750 cal. BP) was identified at 343 cm depth. Leaves, found at 365 cm depth, gave a ^{14}C age of 10,850 ± 170 cal. BP. This age marks a rapid increase of C_{org} content from 0.5 to 3 wt%. C_{org} content remains relatively high throughout the Holocene, indicating establishment of Magellanes rainforest. At around 400 cm core depth, a relatively high Late Glacial percentage of clay fraction (40–45 vol%) changes to lower values (25–35 vol%; Fig. 4C) and Al_2O_3/TiO_2 ratios drop significantly. This marks the change from more allochthonous to predominantly autochthonous sedimentation which persisted throughout the Holocene (Fig. 4C). Foraminifers or other biogenic carbonate components were not detected by systematic investigation with the SEM. The Holocene sedimentation rates are in the range of 0.34–0.46 mm/yr (Fig. 4C). Assuming a similar sedimentation rate of 0.5 mm/yr for the Late Glacial, the change from allochthonous to predominant autochthonous sedimentation at 400 cm depth occurred at around 11,550 cal. BP. An ice rafted debris (IRD) layer was found between 415 and 443 cm core depth, suggesting a formation at around 13,000 cal. BP or even younger, in case sedimentation rates were higher than assumed. This IRD layer indicates the glacial retreat from glacier limit D (Fig. 2) between 15,000 and 12,000 cal. BP (Kilian et al., in press).

The clayey to silty SK1 sediment core from eastern Seno Skyring does not contain any macroplant remnants or biogenic carbonates for ^{14}C determination. Organic carbon content is lower than 1.5 wt% and was considered as not suitable for ^{14}C dating. However, four tephra layers were identified and represent good time markers (Kilian et al., 2003; Table 1). The Aguilera tephra was identified in 82–84 cm depth (<3620 cal. BP; Fig. 4D), a prominent tephra of Mt. Burney was detected in 96–118 cm depth (4290 cal. BP). Another early Holocene tephra layer of Mt. Burney volcano at 192–195 cm depth (8750 cal. BP) and a tephra layer of Reclus volcano at 356–358 cm depth (16,000 cal. BP) were found. These ages constrain relatively low sedimentation rates between 0.17 and 0.22 mm/yr, with lowest rates of 0.17 mm/a during the Holocene climate optimum between 9000 and 4500 cal. BP (Fig. 4D). An IRD layer with lithic grains >2 mm was found at 420 cm core depth. Assuming similar sedimentation rates of 0.22 mm/a below the Reclus tephra layer (Fig. 4D), the IRD layer was formed at around 18,000 cal. BP.

The clay fraction (0.5– μm) is roughly positively correlated with MgO contents, Al_2O_3/TiO_2 ratios and chlorite contents (Fig. 4D). The clay fraction of the superficial sediment consists of 52% vermiculite, 19% illite, and 30% chlorite. Between 16,000 and 13,000 cal. BP the sediment has the highest contents of clay, chlorite (~59% chlorite in the clay fraction) and MgO, and high Al_2O_3/TiO_2 ratios. Systematic investigations with the scanning electron microscope show that the SK1 sediment core includes diatoms, but no biogenic carbonate (e.g. foraminifers). This suggests a limited salinity (<23–26‰; Cronin et al., 2000) in the Seno Skyring ever since 18,000 cal. BP.

4.3. Thermohaline characteristics

The summer–winter depth profiles (Fig. 6) of station CT1 in the Swett Channel (for location see Fig. 3), located near the glacial melt water plumes of GCN, show a seasonally independently stratified water column with respect to salinity and oxygen content. From this station towards the west, the 45 km long Profile 1 (7 measurement stations; Fig. 7) was measured along Seno Glacier and Bahia Beaufort (profile orientation in Figs. 2 and 3). Lowest salinities of 5–25‰ occur in a 20 m thick surface layer of the easternmost section of Profile 1 (Fig. 7), where the superficial glacial melt-water input is most pronounced. From there towards Bahia Beaufort and the western entrance of the Strait of Magellan the surface salinities increase to >26‰ (Fig. 2).

In the southeastern Seno Glacier area, the low salinity surface layer (<28‰) reaches 30 m thickness, due to the predominant westerly winds (see arrows in Figs. 2 and 3). Towards the west and opposite to the predominant wind direction this layer thins to <12 m at the entrance of Bahia Beaufort (Fig. 7). However, the surface layer above the 30‰ salinity isoline remains 50–60 m thick throughout the whole profile, indicating that only the upper 20–30 m are thickened towards the east by wind stress (Valle-Levinson et al., 2001; Valle-Levinson and Blanco, 2004).

CTD Profile 1 indicates inflow of water with relatively high salinities (>32‰), low oxygen contents of >7 ml/l and intermediate temperatures of 9–10 °C from the Strait of Magellan into Bahia Beaufort at intermediate water levels between 100 and 250 m (see arrow in Fig. 7). The lowest oxygen levels of 6–7 ml/l occur in the innermost fjord section of the Swett Channel at depths greater than 50 m below the glacial melt water fan, where biogenic productivity and resulting oxygen consumption may be low (Escribano et al., 2003; for location see Figs. 2 and 3). This indicates low recharge rates with Pacific water for this low oxygen bottom water.

Thermohaline characteristics and oxygen contents of the 200 m deep semi-closed pro-glacial Glacier Bay (Fig. 3) and its <25 m deep sill towards the deeper fjord system are illustrated in Profile 2 (Fig. 8). There is a net superficial outflow (uppermost 10–15 m) of relatively cold <6 °C and low salinity water (<17‰) which transports most of present day glacial clay from GCN into Swett Channel area (Fig. 3). An inflow of warmer (10 °C) water with higher salinity (25–28‰) occurs in the very restricted depth interval of 10–20 m. However, deeper parts of the basin (>80 m water depth) show salinities higher than 30‰ and are accompanied by very low oxygen contents (<5 ml/l). In Swett Channel outside of the 25 m deep shallow sill, similar salinities of >30‰ are reached only at a water depth of 55 m (Figs. 6 and 8).

The CT2 station in the middle section of Seno Sykring (437 m water depths) shows most similar summer and winter depth profiles for salinity and oxygen between 75 and >400 m water depth (Fig. 6). In the upper 75 m of the water column temperatures follow the seasonal course, while salinity (17–18‰) shows only little seasonal changes. Profile 3 (Fig. 9) illustrates that the superficial low salinity layer is 5–25 m thick in the north-western Gajardo Channel and western part of Euston Channel. Towards the easternmost Skyring this layer thickens to approximately 50 m.

The bottom water of Seno Skyring (below 50 m water depths) is characterised by salinities of 19–19.5‰, low oxygen contents of 6–7 mg/l and low temperatures of

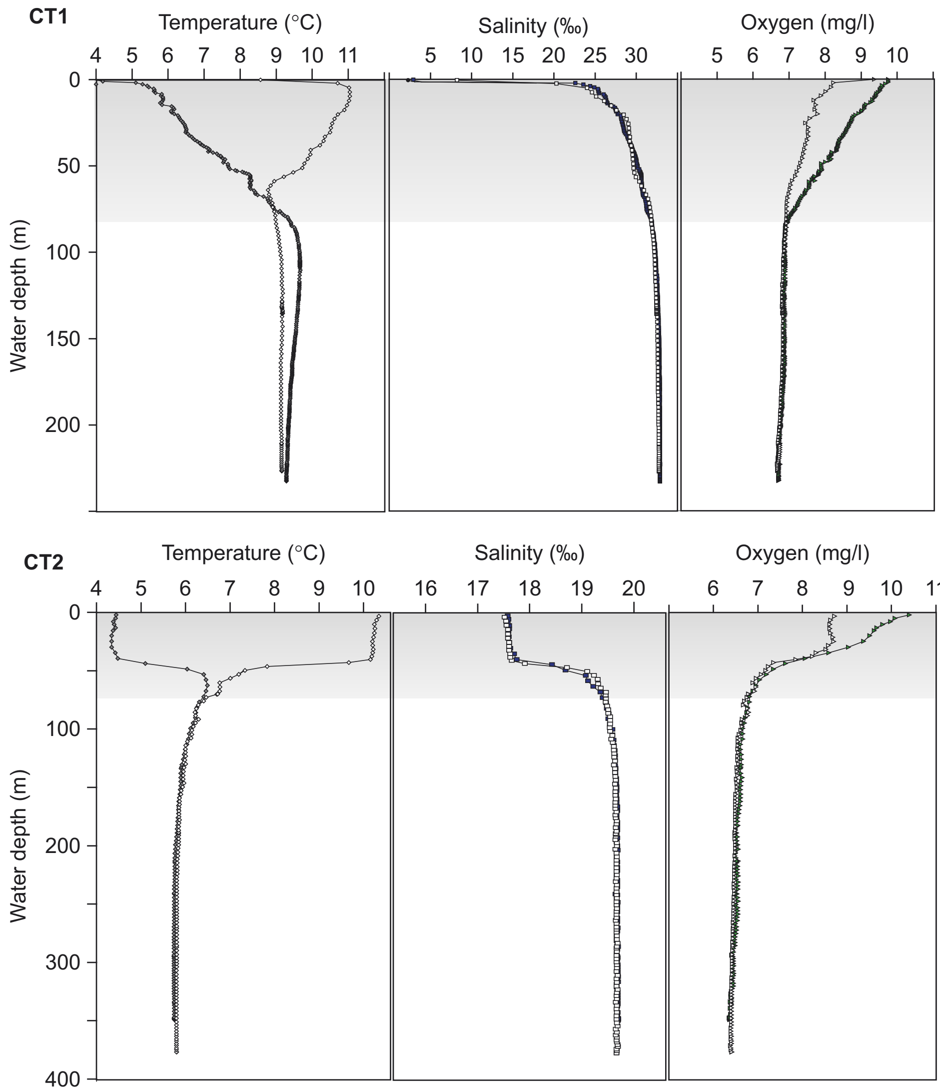

Fig. 6. Comparison of winter and summer profiles for temperature, salinity and oxygen from CT1 station (upper) in Swett Channel (for locations see Figs. 1 and 2) in winter (20.9.2004; filled symbols) and summer (6.3.2005; open symbols) and from CT2 station (lower) from Seno Skyring (for location see Fig. 1) also measured in winter (31.8.2004; filled symbols) and summer (12.3.2005; open symbols).

around 6 °C which corresponds to the average annual temperature at sea level of this area (Fig. 9; Schneider et al., 2003). Somewhat higher salinities (20‰) occur at the bottom of Gajardo Channel and are accompanied by relatively higher oxygen contents (7–8 mg/l). Weaker gradients for the depth-related increase of salinity and the decrease of oxygen content from the Gajardo sill (Angostura Tempanos; AT in Fig. 2) towards the 600 m deep northern Gajardo and western Euston Channel are obvious in Profile 3 (see arrow in Fig. 9).

To the east of CT2 station Seno Skyring is crossed by a submarine ridge (80–90 m water depths; Figs. 2 and 9). A 220 m deep basin located to the east of this ridge shows the highest bottom water salinities (>21‰) of the Seno Skyring fjord system. These lead to the highest salinity gradient towards the surface layer (17.5–18.0‰; Fig. 9). In addition, there are relatively low oxygen contents in this bottom water (~6.5 ml/l) and very high gradients towards the oxygen-rich surface layer (>9 mg/l). These high gradients indicate very low exchange between bottom water and the surface layer in eastern Seno Skyring. In the easternmost shallow section (<50 m water depth) of Seno Skyring, wind- and tide-induced turbulences prevent the formation of a stratified water column.

5. Discussion

5.1. Marine transgression and estuarine development since the LGM

The marine transgression into the fjord system of the Southern Andes was controlled by the relationship between sea level rise (Fig. 5; e.g., Fairbanks, 1989; Bard et al., 1996; Clark et al., 2004; Rohling et al., 2004), tectonic vertical movements (Bentley and McCulloch, 2005) and isostatic uplift of the Andes (Porter et al., 1984; McCulloch

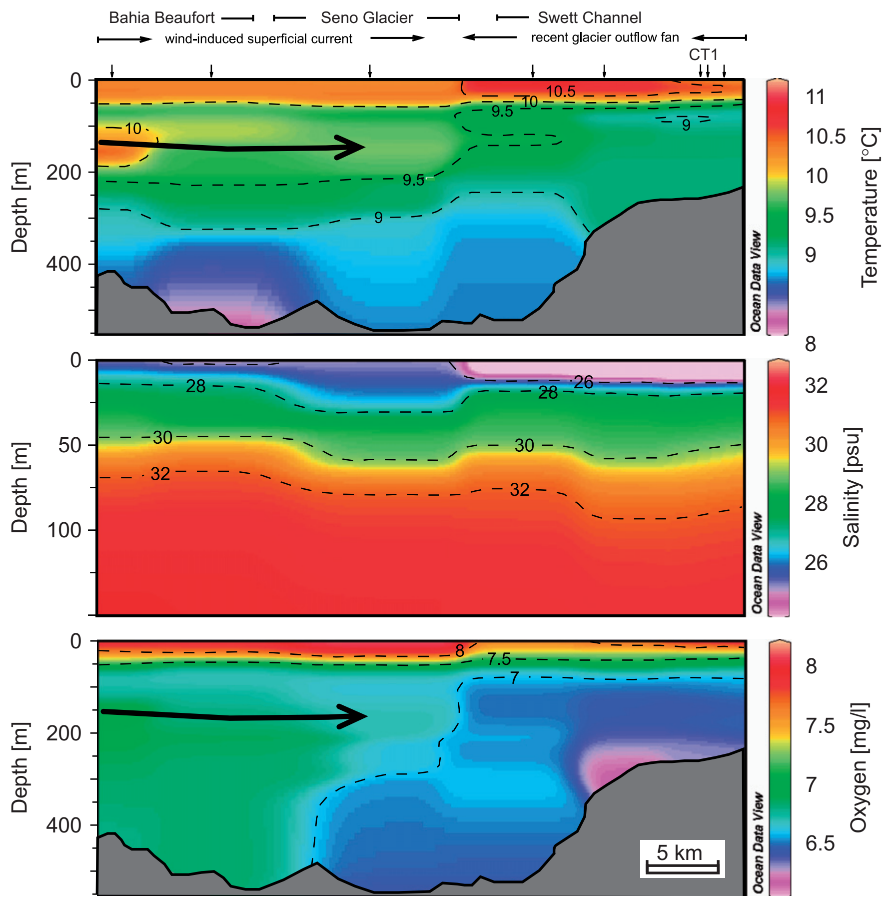

Fig. 7. Thermohaline characteristics and oxygen contents of Profile 1 (for location see Fig. 1). The 43 km long profile was taken from March 6 to 8, 2005 and produced with the Ocean Data View Programme by Schlitzer (2004) from 7 CTD stations indicated by vertical arrows on top. The temperature profile is shown only for the upper 200 m where pronounced changes occur. *Note*: Typical winds move superficial low salinity water to the southeastern section of the profile (middle part of the profile). Dark thick arrows indicate inflow of mixed Pacific water at intermediate levels in 100–200 m water depth.

et al., 2005b), which is still poorly constrained. Glacio-isostatic rebound is typically restricted to previously glaciated areas (Hulton et al., 1994; Larsen et al., 2004), so that the western entrance of the Strait of Magellan and Fitz Roy Channel (Fig. 1) were probably little affected by glacio-isostasy, while the GCN area suffered pronounced isostatic uplift.

A strong increase in C_{org} and biogenic carbonate content (>10 wt%), together with first appearance of foraminifers, occurred synchronous in the sediment cores PAR1 and TM1 between 14,500 and 13,500 cal. BP (Figs. 4A, B and 5). These changes can be explained by an increased salinity and marine bioproductivity. During this phase both sediment cores also show very high Fe_2O_3/TiO_2 ratios and pronounced sulphur peaks, caused by high precipitation rates of Fe sulfides (as pyrite) and hydroxides, due to an increase in salinity and pH.

TM1 shows a pronounced increase of biogenic carbonate which culminates at first at around 14,000 cal. BP and later at around 12,000 cal. BP (Fig. 5B). These changes are produced by changes in the accumulation rates of benthic forminifera and may be related either to changes in water temperature or salinity. In PAR1 changes in biogenic carbonate are related especially to the deposition of shell-rich sandy layers which represent reworked shells from near beaches. At the shallow site inside of a bay these sand layers could have been deposited during lowering of the coastline (sea level changes and/or tectonic subsidence) or by Tsunamis or storm events.

The marine transgression may have occurred especially during melt water pulse 1A which caused a sudden sea level rise from –95 to –70 m NN between 14,300 and 13,800 cal. BP (Fig. 5; e.g. Fairbanks, 1989; Bard et al., 1996; Rohling et al., 2004). This led to floating of the sill of the western Strait of Magellan towards the Pacific which has present-day water depths of 60–80 m (SHOA, 1999). This marine incursion was much earlier than in the central section of the Strait of Magellan near Puerto del Hambre, where glaciers from Cordillera Darwin locked the Strait of Magellan and a proglacial lake persisted until at least 12,200 cal. BP (McCulloch et al., 2005b).

Late Glacial (~15,000 cal. BP) clayey sediments from TM1 and PAR1 have andesitic composition and intermediate Al_2O_3/TiO_2 ratios (18–22). Such clayey sediments

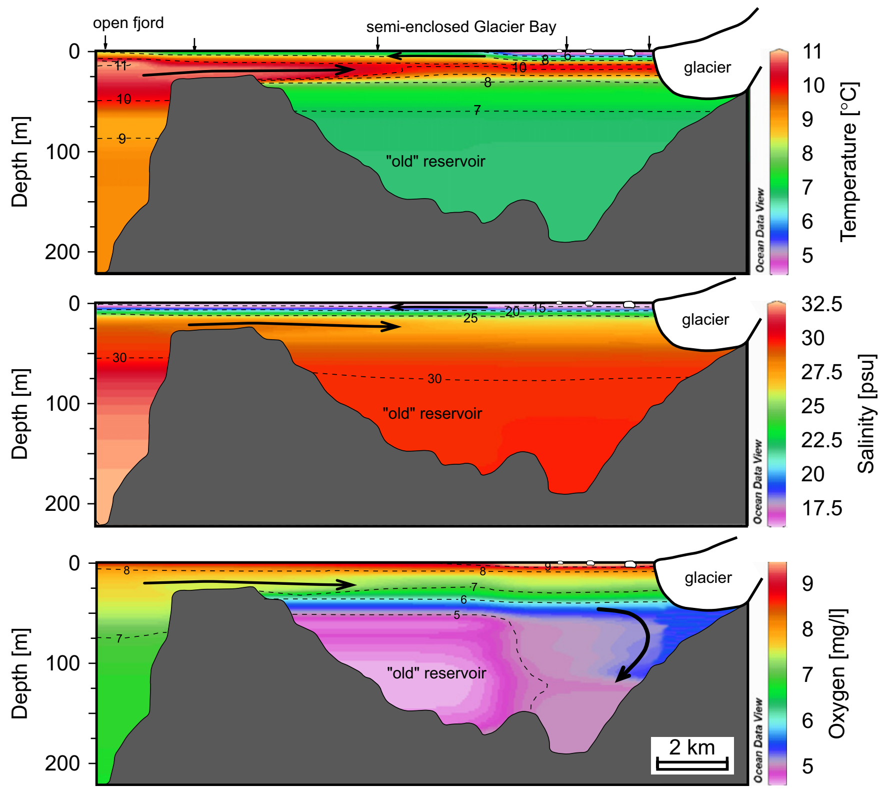

Fig. 8. Thermohaline characteristics and oxygen contents of Profile 2 (for locations see Figs. 2 and 3), reaching from semi-enclosed Glacier Bay across a 25 m deep sill to the deeper fjord section. The profile was taken on March 10, 2005 and produced with the Ocean Data View Programme from Schlitzer (2004) from 5 CTD stations indicated by vertical arrows on top. Arrows in the water body indicate possible currents discussed in the text.

are typical for sediments originated from rocks of the Patagonian Batholith exposed at GCN and indicate a predominant allochthonous origin of the Late Glacial sediments in the Western Strait of Magellan (Fig. 1). The first appearance of foraminifers at around 14,000 cal. BP (arrow in Fig. 5B) indicates an increase of salinity to >26‰ (e.g. Cronin et al., 2000), which could have also triggered flocculation and faster settling of clay minerals (e.g. McCool and Parsons, 2004) in the glacial melt water plumes of the GCN area, so that these sediments did not reach Parker Island anymore. Late Glacial and Holocene sedimentation rates decrease strongly from Swett Channel near to Gran Campo (0.7–2.6 mm/yr: deduced from echosounding profiles) towards the more western TM1 (0.2–0.7 mm/yr) and PAR1 sites (0.1–0.4 mm/yr). This indicates also a very restricted sediment transport from glacial melt water plumes of GCN after the marine transgression and during the Holocene.

In TM1 and PAR1 cores the Late Glacial increases in C_{org} accumulation between 14,000 and 12,500 cal. BP was accompanied by increased C/N ratios (Fig. 5A). This indicates that besides marine algae terrestrial plants also have contributed to the increased C_{org} accumulation although temperatures may have been still relatively low during the so-called Antarctic Cold Reversal (ACR: compare Byrd ice core of Fig. 5D).

Extended glaciers (Limit E, Clapperton et al., 1995) have been reported in the Strait of Magellan between 14,000 and at least 11,500 cal. BP (McCulloch et al., 2000; McCulloch and Davies, 2001; Sudgen et al., 2005). Kilian et al. (in press) reported similar but not so extended glacier advances at GCN until around 11,500 cal. BP. The former authors agree that these glacier advances were produced especially by an increased precipitation due to southward migration of the westerlies. The strong drop in C_{org} accumulation in PAR1 and TM1 between 12,500 and 11,000 can be explained by these Late Glacial glacier advances and resulting colder surface water with lower salinities, but also by a more restricted terrestrial vegetation. Near GCN pioneer pollen associations, typical for moraines, were present until around 11,000 cal. BP (Fesq-Martin et al., 2004).

Soon after 11,000 cal. BP pollen records from near to GCN indicate an evolved Magellanes rain forest (Fig. 5G; Fesq-Martin et al., 2004). At the same time C_{org} contents increase again strongly in VO1, TM1 and PAR1 cores. This second C_{org} peak was caused by enhanced production of marine algae (increasing temperature: compare Byrd ice record, Fig. 5D) and by an evolved Magellanic Rain Forest (Fesq-Martin et al., 2004; Fig. 5G).

Between 11,000 and 8000 cal. BP the sediment cores VO1, PAR1 and TM1 show very high C_{org} contents with

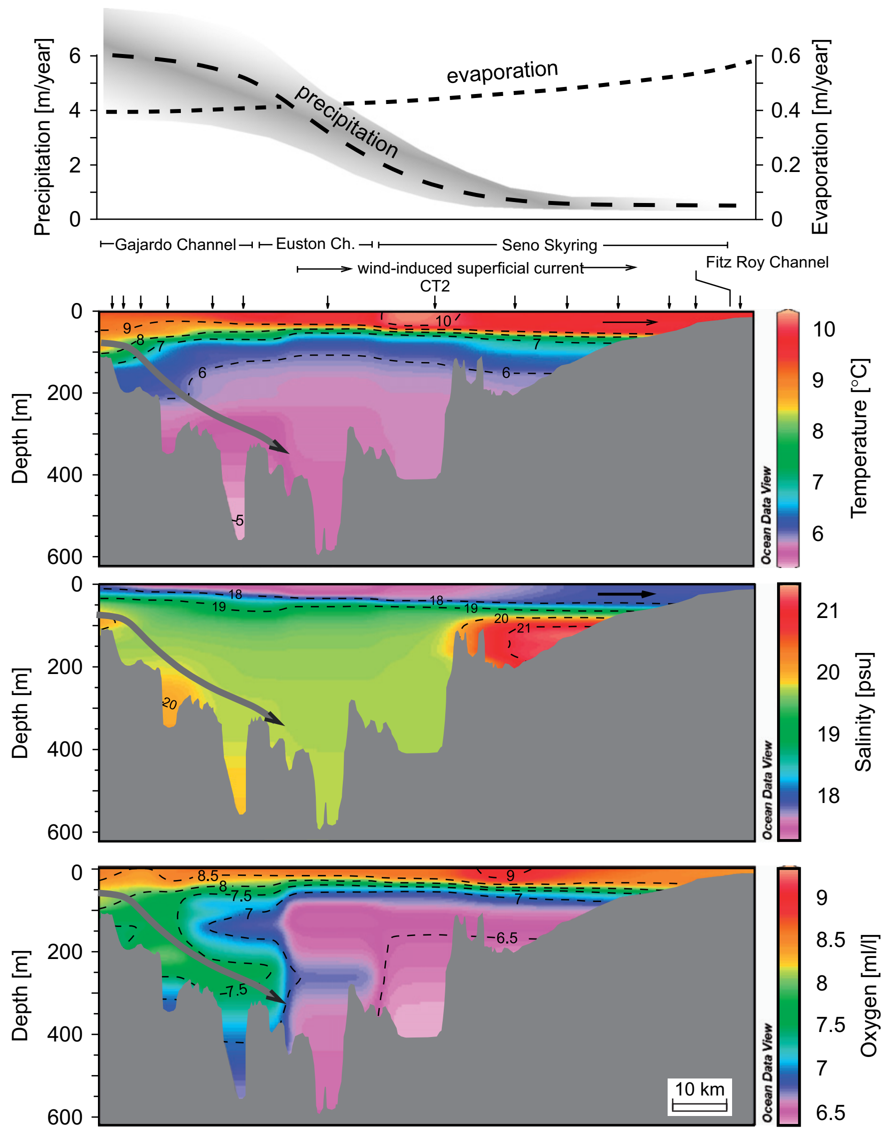

Fig. 9. Thermohaline characteristics and oxygen contents along the 115 km long Profile 3 (for location see Fig. 1) in the Seno Skyring Fjord system with bathymetry from Kilian et al. (in press). The cross-section was taken on March 23, 2005 and produced with the Ocean Data View Programme from Schlitzer (2004) from 14 CTD stations indicated by vertical arrows on top. Black arrows in the water body indicate superficial eastward current and a possible gravity current (left). Changes in annual precipitation along the profile are adapted from Schneider et al. (2003). Annual evaporation was estimated according to Jacobs (1951), quoted in Baumgartner and Reichel (1975).

relatively high C/N ratios (15–19; Fig. 5A), probably due to an expanded early Holocene vegetation. Afterwards, C_{org} contents and C/N ratios decrease strongly in all sediment cores due to the overall cooler climate since the Middle Holocene.

During the Holocene biogenic carbonate content of the TM1 core increased continuously until around 4500 years BP. Since then decreased until the last 1000 cal. BP. This high accumulation of biogenic carbonate (up to 35 wt% $CaCO_3$; predominantly benthic foraminifera) in the Middle Holocene is accompanied by relatively low C_{org} contents with low C/N ratios (Fig. 5A and B). The opposite developments of biogenic carbonate and C_{org} are difficult to explain by climate changes. However, these trends could have been produced during relatively high Middle Holocene sea levels (+6 to +8 m compared to present day sea level; Porter et al. 1984; McCulloch et al. 2005a), which reduced the vegetation area on the islands (leading to lower terrestrial C_{org}) and enabled saltier water of the stratified water column to reach the shallow coastal sites, leading to higher biogenic carbonate productivity.

In Seno Skyring, biogenic carbonate content of sediment cores SK1 and VO1 is very low and foraminifers are absent which indicates only limited salinity (<26‰; e.g. Cronin et al., 2000). This behaviour makes it difficult to constrain the marine transgression to the Skyring fjord system. In SK1 core the glacier retreat from Seno Skyring is marked by an IRD layer at around 18,000 cal. BP (Figs. 4D and 5) leaving behind a proglacial lake. A major glacier recession after LGM was suggested nearly coeval for the Strait of Magellan (McCulloch et al., 2005a; Sudgen et al., 2005).

Marine transgression to Seno Skyring could have occurred either through Jerónimo Channel and Seno Otway and/or through Gajardo Channel (Fig. 1). The above described marine transgression of the western entrance of the Strait of Magellan between 14,500 and 13,500 cal. BP (Fig. 5) was nearly coeval to deglaciation of the Jerónimo Channel (Fig. 1; >80 m water depths at present) at 14,600 ± 420 cal. BP (Table 1; Mercer, 1970). Due to the opening of Jerónimo Channel the water level of proglacial lakes Otway and Skyring (Fig. 1; marked by 25 m high Late Glacial terraces along both Senos) were lowered rapidly and vegetation started to grow in the former easternmost spillway of Seno Otway towards the Atlantic (minimum age constraint of Mercer, 1970). At that time Seno Skyring remained a proglacial lake with drainage through Fitz Roy Channel (10 m water depth at present) towards Seno Otway (Fig. 1).

Chlorite-rich sediments (59% chlorite and 41% illite) were found in association with the mafic to intermediate Jurassic to Cretaceous lithologies northeast of GCN along the major ancient glacier beds in Northern Gajardo Channel and also in Estero Vogel (coring site VO1; for location see Figs. 1 and 2). SK1 and VO1 cores (Fig. 4C and D) indicate that high amounts of such chlorite-rich glacial clay were transported from GCN and Ladrillero areas towards the eastern Seno Skyring between 16,000 and 13,000 years, indicating a still extended glaciation in the Cordillera (glacier limit D in Fig. 2). Long distance transport of glacial clay-bearing meltwater plumes from the GCN area towards the east is explained by fast wind-induced eastward superficial currents and/or slow clay settling rates due to limited flocculation in the lacustrine environment (e.g. Van Leussen, 1999). At around 13,000 cal. BP long-distance clay transport (>80 km) from GCN to eastern Seno Skyring slowed down significantly, as can be deduced from decreases in the contents of MgO and chlorite and Al_2O_3/TiO_2 ratios in SK1 core (Figs. 4D and 5E). This indicates the retreat of GCN glaciers from limit D to E (Fig. 2; Kilian et al., in press).

The SK1 core indicates that the eastward far-distance transport of Andean clay decreased more or less continuously since the Late Glacial and throughout the Holocene (Figs. 4D and 5E). One reason could be that suspended solid concentration in the superficial water of the Andean fjord section became lower, due to continuous glacier retreat. But as discussed above this is only a likely scenario for the period between 12,000 and 11,000 cal. BP. A pollen record from a site near GCN indicates an evolved Magellan Rain Forest after around 10,800 cal. BP and throughout the Holocene (Fig. 5G; Fesq-Martin et al., 2004). Several global climate records (e.g. Dahl and Nesje, 1996; Marchal et al., 2002; Ninnemann et al., 1999), the oxygen isotope record from Byrd ice core (Fig. 5D; Blunier and Brook, 2001) and regional climate reconstructions (Fesq-Martin et al., 2004; Koch and Kilian, 2005; Kilian et al., in press) indicate that the climate became generally colder and more unstable throughout the Holocene after around 8000–7000 cal. BP culminating in the Little Ice Age. Such a cooling trend would have enhanced the clay mobilisation in the Andes, due to glacier advances and perturbation of the vegetation cover, but the reverse was observed in SK1 core. As discussed above, shallowing of the sills during the Holocene led to decreasing salinity in the Seno Skyring fjord system. The salinity influences clay flocculation and settling rates (Van Leussen, 1999). However, different investigations do not give a consistent view on the importance of salinity for sedimentation rates (e.g. Dyer, 1989; Eisma, 1993). The decreasing salinity in the Skyring Fjord system could have led to less flocculation and to increased far-distance clay transport during the Holocene, which is opposite to the implications from the SK1 core.

Typical clay settling rates are in the range of 2–16 m per day (Aston, 1978; Dyer, 1989; Van Leussen, 1999). Periods with strong winds of 15 m/s are frequent in the open and wind channelised Seno Skyring fjord. These conditions would lead to a superficial water flow of around 0.3 m/s, like observed in the comparable Alaskan Puget Sound (Matsuura and Cannon, 1997). Such a superficial current would need 3 days for the 80 km from Gajardo Channel to eastern Seno Skyring. This is not enough time for most clay minerals to sink down into the more stable water column below 30 m depth, especially if the turbulent shear stress hampers flocculation or destroys clay flocs (e.g. Dyer, 1989). Among the discussed influences on clay settling, wind is likely to be the most important factor which controlled the far-distance sediment transport in Seno Skyring. During the Holocene, a decreasing content of Andean clay in the SK1 sediment core can be explained by a decline in average westerly wind velocities due to a northward shift of the westerlies, caused by a global cooling trend after ~8000 cal. BP (Fig. 5E). A northward shift of the westerlies since around 7000 cal. BP was also suggested by Lamy et al. (1999, 2004; see also Fig. 5F5). Drier conditions at 53°S (GCN) due to less westerly influence were also suggested for the Neoglacial of the last 4000 years by Koch and Kilian (2005), because Neoglacial glacier advances at GCN were not as pronounced as further to the north in the Patagonian Andes.

The transition from glacial clay to organic-rich sediments in a sediment core from a small lake on Chandler Island in the Gajardo Channel (CH1 in Fig. 2) was dated to 12,110 ± 190 cal. BP (Kilian et al., in press) and indicates that glaciers retreated from the Gajardo Channel and glacier limit E (Fig. 2) between 12,200 and 11,000 cal. BP. This led to the opening of the shallow sill of Angostura Tempanos in the Gajardo Channel which connects the Seno Skyring fjord system with the Strait of Magellan at present. Near to GCN, glacier loading at that time may have had depressed the crust more than global sea level depression and may have enabled marine transgression to Seno Skyring after ice retreat from Gajardo Channel at around 11,000 cal. BP.

During the Holocene the regional uplift near GCN was faster than the global sea level rise, as the following observations indicate: At the shores of Bahia Bahamondes in Gajardo Channel (10 km northwest of AT in Fig. 1) marine sediments, found on a 8–10 m high terrace above present day sea level (Hohner, 2001), are intercalated with tephra deposits of the 4290 cal. BP eruption of Mt. Burney (Kilian et al., 2003). This suggests a 8–10 m higher paleo-coastline at around 4300 cal. BP (Fig. 5). In a sediment core from the small Martillo Lake (MA1 in Fig. 2) in Bahia Bahamondes a change from marine to lacustrine sedimentation occurred at around 5550 cal. BP (Baeza, 2006). At present, the discharge of this lake is 17 ± 2 m above sea level, which suggests a ~20 m higher coastline at that time. On Chandler Island in the Gajardo Channel sediments of a small lake (coring site CH1 in Fig. 2) have been drilled and investigated (Kilian et al., in press). At present, the discharge of this lake is 37 ± 5 m above sea level. The 6.5 m long sediment core shows lacustrine sedimentation since at least 12,200 cal. BP (Kilian et al., in press). These findings constrain the Andean uplift near GCN and indicate that the Gajardo Channel was uplifted at least approximately 20 m during the Holocene with respect to global sea level rise. This would have enabled much higher influx of saline Pacific water through the Angostura Tempanos during the Early to Middle Holocene. Previously higher recharge rates with saline water could explain the formation of the "old" bottom water with relatively high salinity (>21‰) and oxygen in the eastern Seno Skyring (Fig. 7). However, no foraminifers were found in VO1 and SK1 sediment cores, so that the Late Glacial and Holocene salinities of Seno Skyring did not exceed 26‰ (Cronin et al., 2000).

During the Holocene recharge of marine water to Seno Skyring occurred especially through Angostura Tempano. At present, there is a 50 m wide tidally controlled channel at Angostura Tempanos with 3–5 m water depth, which enables inflow of 100–200 $m^3 s^{-1}$ during approximately 8 h per day (maximum of $10^8 m^3 a^{-1}$; Marangunic et al., 1992). Assuming such an inflow rate, it would take approximately 500 years just to fill up the $70\times10^{10} m^3$ water volume of the Seno Skyring fjord system. However, large amounts of water which enter through the Angostura Tempanos by tidal currents do not enter permanently, but rather are removed backwards during low tides. It is difficult for saline water to pass such shallow sills without mixing with superficial freshwater (Valle-Levinson et al., 2001). Thermohaline Profile 3 (Fig. 9) indicates that at present only small amounts of water with sufficiently high salinity pass Angostura Tempanos, so that only a weak gravity current enters Gajardo Channel. Thus the recharge of Seno Skyring with marine water is not efficient.

5.2. *Thermohaline, tidal and wind-influences on fjord currents*

Estuarine fjord systems show complex properties for mixing between marine and freshwater (e.g. Valle-Levinson and Blanco, 2004). However, despite influences by tides and strong westerly winds, thermohaline profiles from the western section of the fjord transect are well stratified whole-year-round (Figs. 7–9), as also has been reported previously for the western Strait of Magellan by Panella et al. (1991). Stratified water with salinities of around 33.7‰ at a water depth of 50 m were observed as far as 75 km offshore in the Pacific (Dávila et al., 2002).

CTD Profile 1 shows that still mixed Pacific water (with salinities of 32‰) enters the Bahia Beaufort and Seno Glacier Fjord system in an intermediate layer (100–200 m water depth; Fig. 7). Tides in this fjord transect may cause partial mixing between saltier Pacific water and freshwater even in the deeper parts of the water column in the fjords near GCN. However, salinities of >32‰ were measured below the superficial glacial melt water plume in the Swett Channel (Figs. 7 and 8).

In sill-protected deeper bays, like Glacier Bay (Fig. 8; for location see Fig. 3), bottom water with relatively high salinities (>30‰) are not in equilibrium with typical present day in- and outflow characteristics. However, recharge of saline water could have occurred during rare extremely dry and wind-poor climate events in winter (Stanton, 1986) which enable saline Pacific water to reach higher levels in the water column. However, it is more likely that such high salinity bottom water has been formed much earlier during the Holocene, when the GCN area was around 20 m lower with respect to paleo-sea level (Fig. 5) and inflow rates across sills might have been much higher (<10 fold).

The thermohaline Profile 1 (Fig. 7) indicates that the week westward outflow of superficial freshwater is restricted by the westerlies which move the uppermost 10–30 m of the water column against the general outflow direction. This seems to also prevent westward migration (<25 km) of the thin superficial clay-rich glacial melt water plumes derived from the GCN (Fig. 3) and can explain the relatively low sedimentation rates of PAR1 (0.1–0.4 mm/yr; Fig. 4A) in the Western Strait of Magellan at least since the marine transgression between 14,500 and 13,500 cal. BP.

The westernmost Skyring area is affected by annual precipitation sums of 4000–7000 mm/yr (Schneider et al., 2003) and a most likely annual freshwater addition of 20–30 m, while in the eastern section of Seno Skyring the amount of annual precipitation is less than 600 mm, evaporation is relatively high (Fig. 9; 350–600 mm/yr) and freshwater input by river systems is very limited. However, the uppermost layer of low salinity reaches only 5–25 m thickness in the north-western Gajardo Channel and the western part of Euston Channel (Fig. 9). Towards the eastern Seno Skyring and the sill of Fitz Roy Channel, associated with the predominant westerly wind direction (annual wind speed of approximately 4 m/s with frequent periods of wind speed in excess of 15 m/s; Schneider et al., 2003), the surface layer of low salinity increases to approximately 50 m in thickness (Fig. 9). These considerations and wind-dependent lake levels of the Seno Skyring fjord system indicate that superficial freshwater is transported very effectively by the westerlies to eastern Seno Skyring and pushed out through the Fitz Roy Channel (Fig. 2). Such a process could lead to up-welling in the western part of the fjord system (Kiiriki and Blomster, 1996; Asplin et al., 1999), but the relatively high precipitation throughout the whole year in the western Skyring area seems to prevent this.

6. Conclusions

Four sediment cores from a transect of the southernmost Andes at 53°S indicate an early and fast ice retreat after the LGM, starting before 18,000 cal. BP and leaving behind extended proglacial lakes. Marine transgression to the Western Strait of Magellan occurred between 14,500 and 13,500 cal. BP and is characterised by strongly increased accumulation of terrestrial and aquatic C_{org}, biogenic carbonate with foraminifers, precipitation of Fe sulfides and hydroxides, and decreasing sedimentation rates. After ~11,500 cal. BP and throughout the Holocene, sedimentation in the western fjords became predominantly autochthonous due to higher salinity and clay flocculation, and restricted extend of GCN glaciers. During the Holocene sedimentation rates in the fjord system show a strong gradient from the GCN at the climate divide (>1 mm/yr) towards the Western Island Zone of the continental margin (<0.1 mm/yr). Present day CTD profiles indicate that the uppermost 20–30 m thick layer is strongly wind-influenced and year-round westerlies limit westward transport of clay from glacial melt water plumes, as also indicated by sedimentological data. The tidally influenced western fjords show partially mixed thermohaline characteristics, indicating limited exchange between Pacific water and freshwater. These fjords show a generally well stratified water column. The surface salinities control accumulation of biogenic carbonate.

During the Late Glacial to early Holocene, marine transgression to semi-haline fjords (<20‰ salinity) such as Seno Skyring may have occurred very slowly. In the GCN area significant Late Glacial glacier retreat occurred between 12,000 and 11,500 cal. BP and opened pathways for the marine transgression, such as the Gajardo Channel, which had been significantly depressed due to glacier loading. As a result of the delayed isostatic uplift of the Andes compared to global sea level rise, sills became shallower throughout the Holocene which led to a more and more restricted exchange between marine and freshwater. Due to high annual precipitation in the Andes, strong pycnoclines were formed and hampered the exchange across the shallow sills. Thus, Seno Skyring represents a fjord system which is not in equilibrium with present day in- and outflow characteristics and has stored ca. 2000-year old marine water. The 100 km long and W–E-oriented fjord system of Seno Skyring has a pronounced eastward, wind-induced superficial current. While the Late Glacial long distance sediment transport from the Andes to eastern Seno Skyring was controlled by deglaciation and related glacial clay input, the decreasing amount of eastward transported clay during the Holocene is best explained by decreasing westerly wind influence due to a general northward migration of the westerlies related to the overall Holocene cooling trend.

Acknowledgements

This study was funded by Grant Ki-456/8 of the German Research Foundation (Deutsche Forschungsgemeinschaft: DFG). We are most thankful for constructive comments and suggestions of two anonymous reviewers and Bernd Zolitschka. We also thank Katrin Becker for processing of the bathymetrical map and all sponsors of RV *Gran Campo II*.

References

Acha, E.M., Mianzan, H.W., Guerrero Favero, M., Bava, J., 2004. Marine fronts at the continental shelves of austral South America: Physical and ecological processes. Journal of Marine Systems 44, 83–105.

Anderson, D.M., Archer, R.B., 1999. Preliminary evidence of early deglaciation in southern Chile. Palaeogeography, Palaeoclimatology, Palaeoecology 146, 295–301.

Appleby, P.G., Oldfield, F., Thompson, R., Huttunen, P., Tolonen, K., 1979. ^{210}Pb dating of annually laminated lake sediments from Finland. Nature 280, 53–55.

Arntz, W., Ríos, C., 1999. Magellan-Antarctic: ecosystem that drifted apart. Scientia Marina 63 (Suppl. 1), 518.

Asplin, L., Salvanes, V.A.G., Kristoffersen, J.B., 1999. Nonlocal wind-induced fjord-coast advection and its potential effect on plankton and fish recruitment. Fish Oceanography 8 (4), 255–263.

Aston, S.R., 1978. Estuarine chemistry. In: Riley, J.P., Chgester, R. (Eds.), Chemical oceanography, vol. 7. Academic Press, New York, London, pp. 361–440.

Baeza, O., 2006. Lake and fjord sediments as Late Glacial to Holocene environmental and climate archives of the southernmost Andes at 53°S, Chile. Inaugural-Dissertation, University of Freiburg, Germany, 262pp.

Bard, E., 1988. Correction of accelerator mass spectrometry 14C ages measured in planktonic foraminifera: paleoceanographic implications. Paleooceanography 3, 635–645.

Bard, E., Hamelin, B., Arnold, M., Montaggioni, L.F., Cabioch, G., Faure, G., Rougerie, F., 1996. Deglacial sea level record from Tahiti corals and the timing of global meltwater discharge. Nature 382, 241–244.

Baumgartner, A., Reichel, E., 1975. The World Water Balance. Elsevier, New York, p. 179.

Bentley, M.J., McCulloch, R.D., 2005. Impact of neotectonics on the record of glacier and sea level fluctuations, Strait of Magellan, Southern Chile. Geografiska Annaler 87A (2), 393–402.

Blunier, T., Brook, E.J., 2001. Timing of millennial-scale climate change in Antarctica and Greenland during the Last Glacial period. Science 291, 109–112.

Biester, H., Kilian, R., Hertel, C., Mangini, A., Shotyk, W., Schöler, H.-F., 2002. Elevated mercury concentrations in South Patagonian Peat Bogs—an anthropogenic signal? Earth Planetary Science Letters 201, 609–620.

Brambati, A., 2000. Palaeoclimate and paleoenvironmental records in sediments from the Southern Ocean (Strait of Magellan and Ross Sea). Terra Antarctica Reports 4, 1–41.

Clapperton, C.M., Sudgen, D.E., Kaufmann, D., McCulloch, R.D., 1995. The Late Glaciation in central Magellanstrait, southernmost Chile. Quaternary Research 44, 133–148.

Clark, P.U., McCabe, M.A., Mix, A.C., Weaver, A.J., 2004. Rapid rise of sea level 19,000 years ago and its global implications. Science 304, 1141–1144.

Cronin, T.M., Willard, D.A., Karlsen, A., Ishman, S., Verardo, S., McGeehin, J., Kerhin, R., Holmes, C., Colman, S., Zimmermann, A., 2000. Climate variability in the Eastern United States over the past millennium from Chesapeake Bay sediments. Geology 28, 3–6.

Dahl, S.O., Nesje, A., 1996. A new approach to calculating Holocene winter precipitations by combinig glacier equilibrium-line altitudes and pine-tree limits: a case study from Hardangerjokulen, central southern Norway. Holocene 6, 381–398.

Dávila, P., Figueroa, D., Müller, E., 2002. Freshwater input into the coastal ocean and its relation with the salinity distribution off austral Chile (35–55°S). Continental Shelf Research 22, 521–534.

Dyer, K.R., 1989. Sediment processes in estuaries: Future research requirements. Journal of Geophysical Research 94 (10C), 14,327–14,399.

Eisma, D., 1993. Suspended Matter in Aquatic Environments. Springer, Berlin, 315pp.

Escribano, R., Fernández, M., Aranís, A., 2003. Physical–chemical processes and patterns of diversity of the Chilean eastern boundary pelagic and benthic marine ecosystems: an overview. Gayana 67, 190–205.

Fairbanks, R.G., 1989. A 17,000-year glacio-eustatic sea level record: influence of glacial melting rates on the Younger Dryas event and deep-ocean circulation. Nature 342, 637–642.

Fesq-Martin, M., Friedmann, A., Peters, M., Behrmann, J., Kilian, R., 2004. Late Glacial and Holocene vegetation history of the Magellanic rain forest in southwestern Patagonia. Vegetation History and Archeobotany 13, 249–255.

Hagedorn, B., Harwart, S., van der Loeff, M.M.R., Melles, M., 1999. Lead-210 dating and heavy metal concentration in recent sediments of Lama lake (Norilsk Area, Sibiria). In: Kassens, H., Bauch, H.A., Dmitrenko, I., Eicken, H., Hubberten, H.-W., Melles, M., Thiede, J., Timokov, . (Eds.), Land–ocean Systems in the Siberian Arctic: Dynamic and History. Springer, Berlin, pp. 361–376.

Hohner, M., 2001. Tephrochronologie und quartärgeologische Aspekte in den südlichen Anden am Beispiel des Gran Campo Nevado-Gebietes. Diploma Thesis, Department of Geology, University of Freiburg, Germany.

Hollin, J.T., Schilling, D.H., 1981. Mountain glaciers and small ice caps. In: Denton, G.H., Hughes, T.J. (Eds.), The Last Great Ice Sheets. Wiley, New York, pp. 179–206.

Hulton, N., Sudgen, A., Payne, A., Clapperton, C.M., 1994. Glacier modelling and the climate of Patagonia during the last glacial maximum. Quaternary Research 42, 1–19.

Jacobs, W.C., 1951. The energy exchange between sea and atmosphere and some of its consequences. Bulletin of the Scripps Institution of Oceanography 6 (2), 27–122.

Kiiriki, M., Blomster, J., 1996. Wind-induced up-welling as a possible explanation for mass occurrences of epiphytic *Ectocarpus siliculosus* (Phaaeophyta) in the northern Baltic. Properties of Marine Biology 127, 353–358.

Kilian, R., Hohner, H., Biester, H., Wallrabe-Adams, C., Stern, C., 2003. Holocene peat and lake sediment tephra record from the southernmost Andes (53–55°S). Revista Geológica de Chile 30, 47–64.

Kilian, R., Schneider, C., Koch, J., Fesq-Martin, M., Biester, H., Casassa, C., Arévalo, M., Wendt, G., Baeza, O., Behrmann, J., in press. Palaeoecological constraints on Late Glacial and Holocene ice retreat in the Southern Andes (53°S). Global and Planetary Change.

Koch, J., Kilian, R., 2005. Little Ice Age glacier fluctuations at Gran Campo Nevado, southernmost Chile. The Holocene 15, 20–28.

Lamy, F., Hebbeln, D., Wefer, G., 1999. High-resolution marine record of climate change in mid-latitude Chile during the last 28,000 years based on terrigeneous sediment parameters. Quaternary Research 51, 83–93.

Lamy, F., Kaiser, J., Ninnemann, U., Hebbeln, D., Arz, H.W., Stoner, J., 2004. Antarctic timing of surface water changes off Chile and Patagonian Ice Sheet Response. Science 304, 1959–1962.

Larsen, Ch.F., Motyka, R.J., Freymueller, J.T., Echelmeyer, K.A., Ivins, E.R., 2004. Rapid uplift of southern Alaska caused by recent ice loss. Geophysical Journal International 158, 1118–1133.

Mann, K.H., Lazier, J.R., 1996. Dynamics of Marine Ecosystems. Biological–Physical Interactions in the Oceans, second ed. Blackwell, Cambridge.

Marangunic, C., Parraguez, C., Stowhas, L., Lucchini, A., Avila, L., 1992. Informe preliminar de hidrologia. Unpublished Report of Geoestudios Ltda, Santiago de Chile.

Marchal, O., Cacho, I., Stocker, T.F., Grimalt, J.O., Calvo, E., Martrat, B., Shackleton, N., Vautravers, M., Cortijo, E., van Kreveld, S., Andersson, C., Koc, N., Chapman, M., Sbaffi, L., Duplessy, J.-C., Sarnthein, M., Turon, J.-L., Duprat, J., Jansen, E., 2002. Apparent long-term cooling of the sea surface in the northeast Atlantic and Mediterranean during the Holocene. Quaternary Science Reviews 21, 455–483.

Matsuura, H., Cannon, G.A., 1997. Wind effects on sub-tidal currents in Budget Sound. Journal of Oceanography 53, 55–66.

McCool, W.W., Parsons, J.D., 2004. Sedimentation from buoyant fine-grained suspensions. Continental Shelf Research 24, 1129–1142.

McCulloch, R.D., Davies, S.J., 2001. Late-glacial and Holocene palaeo-environmental change in the central Strait of Magellan, southern Patagonia. Palaeogeography, Palaeoclimatology, Palaeoecology 174, 143–173.

McCulloch, R.D., Bentley, M.J., Purves, R.S., Hulton, N.R.J., Sudgen, D.E., Clapperton, C.M., 2000. Climatic interferences from glacial and palaeoecological evidence at the last glacial termination, southern South America. Journal of Quaternary Science 15, 409–417.

McCulloch, R.D., Fogwill, C.J., Sudgen, D.E., Bently, M.J., Kubik, P.W., 2005a. Chronology of the last glaciation in central Strait of Magellan and Bahía Inútil, Southernmost South America. Geografiska Annaler 87A (2), 289–312.

McCulloch, R.D., Bently, M.J., Tipping, R.M., Clapperton, C.M., 2005b. Evidence for Late-Glacial ice dammed lakes in the central Strait of Magellan and Bahia Inútil, southernmost South America. Geografiska Annaler 87A (2), 335–362.

Mercer, J., 1970. Variations of some Patagonian glaciers since the Late-Glacial. American Journal of Science 269, 1–25.

Mercer, J.H., 1976. Glacial history of southernmost South America. Quaternary Research 6, 125–166.

Ninnemann, U.S., Charles, C.D., Hodell, D.A., 1999. Origin of global millennial-scale climate events: constraints from the southern ocean deep-sea sedimentary record. In: Clark, P.V., Webb, R.S., Keigwin, L.D. (Eds.), Mechanisms of Global Climate Change at Millennial Time Scales. Geophysical Monograph, vol. 112. American Geophysical Union, Washington, DC, pp. 99–112.

Panella, S., Michelato, A., Perdicaro, R., Magazù, Dicembrini, F., Scarazzato, P., 1991. A preliminary contribution to understanding the hydrological characteristics of the Strait of Magellan: Austral Spring 1989. Bollettino di Oceanologia Theorica ed Applicata IX (2–3), 107–126.

Parsons, J.D., Garcia, M.H., 2000. Enhanced sediment scavenging due to double-diffusive convection. Journal of Sedimentary Research 70, 47–52.

Porter, S.C., Stuiver, M., Heusser, C.J., 1984. Holocene sea level changes along the Strait of Magellan and Beagle Channel, southernmost America. Quaternary Research 22, 59–67.

Rohling, E.J., Marsh, R., Wells, N.C., Siddall, M., Edwards, N.R., 2004. Similar meltwater contributions to glacial sea level changes from Antarctic and northern ice sheets. Nature 430, 1016–1021.

Schneider, C., Glaser, M., Kilian, R., Santana, A., Butorovic, N., Casassa, G., 2003. Weather observations across the Southern Andes at 53°S. Physical Geography 24, 97–119.

Schneider, C., Schnirch, M., Acuña, C., Casassa, G., Kilian, R., in press. Glacier inventory of the Gran Campo Nevado Ice Cap in the Southern Andes and glacier changes observed during recent decades. Global and Planetary Change.

Schlitzer, R., 2004. Ocean Data View Data. 〈www.awi-bremerhaven.de/GEO/ODV〉.

SERNAGEOMIN, 2003. Mapa Geológico de Chile version digital, escala 1:1.000.000. Publicación Geológica Digital, no. 4, CD-ROM, version 1.0, Santiago de Chile.

SHOA, 1999. Mapa Nautica Evangelistas; 1:65,000. Servicio Hidrográfico y Oceanográfico de la Armada de Chile. Valparaiso, Chile.

Stanton, B.R., 1986. Winter oceanographic observations in some New Zealand fiords. New Zealand Journal of Marine and Freshwater Research 20, 299–314.

Stern, C.R., 1990. Tephrochronology of southernmost Patagonia. National Geographic Research 6, 110–126.

Stern, C.R., 1992. Tefrocronología de Magellanes: nuevos datos e implicaciones. Anales del Instituto de la Patagonia. Series Ciencias Naturales 21, 129–141.

Stern, C.R., 2000. The Holocene Tephrochronology of southernmost Patagonia and Tierra del Fuego. In: Congreso Geológico Chileno, Puerto Varas, vol. 9(2), pp. 77–80.

Stow, D.A.V., Tabrez, A.R., 1998. Hemipelagites: processes, facies and model. In: Stocker, M.S., Evans, D., Cramp, E. (Eds.), Geological Processes on Continental Margins: Sedimentation, Mass-wasting and Stability. Geological Society of London Special Publication, vol. 129, pp. 317–337.

Strub, P.T., Mesias, J., Monteciano, V., Rutllant, J., Salinas, S., 1998. Coastal ocean circulation of western South America. In: Robinson, A.R., Brink, K.H. (Eds.), The Sea, vol. 11. Wiley, New York, USA, pp. 273–313.

Stuiver, M., Reimer, P.J., Bard, E., Beck, J.W., Burr, G.S., Hughen, K.A., Kromer, B., McCormac, G., van der Plicht, J., Spurk, M., 1998. IntCal98 radiocarbon age calibration, 24,000–0 cal. BP. Radiocarbon 40 (3), 1041–1083.

Sudgen, D.E., Bentley, M.J., Fogwill, C.J., Hulton, N.R.J., McCulloch, R.D., Purves, R.D., 2005. Late glacial glacier events in southernmost South America: a blend of 'Northern' and 'Southern' hemispheric climatic signals? Geografiska Annaler 87A (2), 273–288.

Valle-Levinson, A., Blanco, L.J., 2004. Observations of wind influence on exchange flows in a strait of the Chilean Inland Sea. Journal of Marine Research 62 (5), 720–740.

Valle-Levinson, A., Jara, F., Molinet, C., Soto, D., 2001. Observations of intratidal variablility of flows over a sill/contraction combination in a Chilean fjord. Journal of Geophysical Research 106 (C4), 7051–7064.

Van Leussen, W., 1999. The variability of settling velocities of suspended fine-grained sediment in the Ems estuary. Journal of Sea Research 41, 109–118.

Winterwerp, J.C., 1998. A simple model for turbulence induced flocculation of cohesive sediments. Journal of Hydraulic Engineering 36 (3), 309–326.

Wunderlich, J., Wendt, G., 2001. Advantages of parametric acoustics for the detection of the dredging level in areas with siltation. 7. Workshop on Dredging and Surveying, Scheveningen, The Haag, June 7–8, 2001, pp. 1–8.